Kameda *et al. Earth, Planets and Space* (2017) 69:52
DOI 10.1186/s40623-017-0635-1

Earth, Planets and Space

FULL PAPER

Open Access

Alteration and dehydration of subducting oceanic crust within subduction zones: implications for décollement step-down and plate-boundary seismogenesis

Jun Kameda[1*], Sayako Inoue[2], Wataru Tanikawa[3], Asuka Yamaguchi[4], Yohei Hamada[3], Yoshitaka Hashimoto[5] and Gaku Kimura[6]

Abstract

The alteration and dehydration of predominantly basaltic subducting oceanic crustal material are thought to be important controls on the mechanical and hydrological properties of the seismogenic plate interface below accretionary prisms. This study focuses on pillow basalts exposed in an ancient accretionary complex within the Shimanto Belt of southwest Japan and provides new quantitative data that provide insight into clay mineral reactions and the associated dehydration of underthrust basalts. Whole-rock and clay-fraction X-ray diffraction analyses indicate that the progressive conversion of saponite to chlorite proceeds under an almost constant bulk-rock mineral assemblage. These clay mineral reactions may persist to deep crustal levels (~320 °C), possibly contributing to the bulk dehydration of the basalt and supplying fluid to plate-boundary fault systems. This dehydration can also cause fluid pressurization at certain horizons within hydrous basalt sequences, eventually leading to fracturing and subsequent underplating of upper basement rock into the overriding accretionary prism. This dehydration-induced breakage of the basalt can explain variations in the thickness of accreted basalt fragments within accretionary prisms as well as the reported geochemical compositions of mineralized veins associated with exposed basalts in onland locations. This fracturing of intact basalt can also nucleate seismic rupturing that would subsequently propagate along seismogenic plate interfaces.

Introduction

At accretionary margins, incoming sediment on the oceanic plate is successively peeled off and accreted to the overriding plate through tectonic processes such as offscraping or underplating along the plate-boundary décollement. As a result, the uppermost oceanic crust, which is mainly made up of basaltic rock, is eventually directly exposed to the upper plate of the lithified accretionary prism. This eventuality can be explained by duplex underplating due to "décollement step-down" into the ocean-plate basalts, as exemplified by several ancient accretionary prisms (Silver et al. 1985; Kimura and Mukai 1991; Kimura and Ludden 1995). Paleothermal analyses (Matsumura et al. 2003; Ikesawa et al. 2005) and seismic reflection surveys of the modern accretionary margin in the Nankai Trough, southwest Japan (Park et al. 2002), suggest that the site where décollement step-down is initiated almost coincides with the up-dip boundary of the seismogenic zone where great earthquakes repeatedly occur (normally defined as having a temperature range of ~100–150 to ~350 °C; Hyndman 2007). Once such an emplacement of the décollement occurs at a certain depth, the downwards extension of the plate interface is thought to lie close to or within the ocean-plate basalt over a wide range of the seismogenic zone. Accordingly, the alteration and dehydration of the underthrust basalts must be key processes for understanding

*Correspondence: kameda@sci.hokudai.ac.jp
[1] Department of Natural History Sciences, Graduate School of Science, Hokkaido University, N10 W8, Sapporo 060-0810, Japan
Full list of author information is available at the end of the article

the in situ mechanical and hydrological properties of the seismogenic plate-boundary fault. Many researchers have examined the mineral dehydration reactions in incoming sedimentary rocks along the plate interface and the influence of these reactions on seismogenesis (e.g., Saffer and Tobin 2011). Although some have emphasized the importance of dehydration of igneous oceanic crust on seismicity at relatively great depths (>400 °C) (e.g., Peacock and Wang 1999; Hacker et al. 2003), there has been little focus on the alteration and low-grade metamorphism of oceanic crust, even though this is probably the principal process within the seismogenic zone.

Recently, we investigated the mineral composition of ocean-floor basalt in the Shikoku Basin, near the trench axis of the Nankai Trough, and we reported that the uppermost ~40 m of pillow basalt is heavily altered to mafic smectite (saponite), often to the extent of ~20 wt% of the bulk rock (Kameda et al. 2011a). We also addressed the sequential conversion of saponite to chlorite (S–C), which can be a significant source of fluid in the seismogenic zone, providing fluid volumes that are almost one order of magnitude greater than in the overriding sediments. The aim of the present work is to strengthen our previous dataset and to explore the states and pathways of basalt alteration along the plate interface. In particular, our work is directed toward a better understanding of the way in which dehydration proceeds within the seismogenic zone. To these ends, we have examined the whole-rock and clay-fraction mineralogy of several basalt fragments that were subjected to alteration under various temperatures in an ancient subduction zone, and which are now exhumed as members of the ancient Shimanto Belt accretionary complex in southwest Japan. As a result of this work, we are now able to demonstrate the possible connections between basalt dehydration and plate-boundary seismogenesis in a subduction zone.

Geological background and analyzed samples

The Shimanto Belt is a Cretaceous-Tertiary accretionary complex that extends for more than 800 km along the Pacific side of southwest Japan (Taira et al. 1988) (Fig. 1). The complex is divided into northern and southern sub-belts by the Aki Tectonic Line in the Shikoku and Kii regions and by the Nobeoka Thrust in Kyushu (Imai et al. 1971). Radiolarian biostratigraphy indicates that the complex is composed of Cretaceous to late Miocene deposits (Taira et al. 1988). The maximum paleotemperatures in the complex range from ~150 to 350 °C, as inferred from vitrinite reflectance (e.g., Mori and Taguchi 1988; Laughland and Underwood 1993; Sakaguchi 1996; Ohmori et al. 1997; Ohmori 1998; Sakaguchi 1999), illite crystallinity (e.g., Kameda et al. 2011b), and fluid inclusion geothermometry (e.g., Matsumura et al. 2003).

The Shimanto complex contains rocks with two contrasting structural features. Rocks classified as the "coherent unit" are made up mainly of terrigenous sandstone/mudstone turbiditic sequences with well-preserved original sedimentary fabrics. On the other hand, rocks that are classified as highly deformed mélange exhibit a chaotic appearance and contain various types/sizes of rock fragments such as oceanic basalt, pelagic chert, red shale, and hemipelagic shale, enclosed in a matrix of highly sheared black shale (Taira et al. 1988). Most of the mélange in the Shimanto complex is supposed to have formed as a result of tectonic processes near the plate boundary (Kimura et al. 2012 and references therein). Although the mélanges have a chaotic appearance on various scales, one commonly observed feature is a systematic repetition of disrupted ocean-floor stratigraphy; that is, a pile of ocean-floor basalt, pelagic to hemipelagic sediments, and trench-fill terrigenous sediments (Kimura and Mukai 1991; Hashimoto and Kimura 1999; Ikesawa et al. 2005). On the basis of detailed structural observations in the Mugi mélange, Kimura et al. (2012) proposed a model where the mélange was underplated together with a duplex structure that was in the process of formation. Slab-shaped basaltic rocks often occur at the base of each horse in such duplex structures, suggesting a décollement step-down into the oceanic crust.

For the present study, we examined five tectonic mélanges that are representative of the Shimanto complex, and which contain basaltic slabs; from these, we collected samples of pillow basalt. The study areas include the upper sections of the Mugi mélange (MGUB), the lower sections of the Mugi mélange (MGLB) (Ikesawa et al. 2005; Kimura et al. 2012), the Kure mélange (KRB) (Mukoyoshi et al. 2006), the Okitsu mélange (OKB) (Ikesawa et al. 2003; Sakaguchi 1999), and the Makimine mélange (MKB) (Fig. 1). All these mélanges have a late Cretaceous to Paleocene accretionary age (Kiminami et al. 1994), and they are characterized by an absence of pelagic sediment, which suggests that the oceanic plate being subducted at that time was relatively young (<20 Myr). This plate tectonic setting is similar to that of the modern Nankai Trough.

Descriptions of the analyzed samples are given in Table 1. The basalts sampled have been subjected to alteration under a wide range of temperatures. The maximum paleotemperature for each sample was estimated from the reported vitrinite reflectance values (Ro) in accompanying terrigenous rocks (Ohmori 1998) (Table 1). Values of Ro were converted to paleotemperatures using equations from Barker (1988) and Sweeney and Burnham (1990) (heating durations of 1 Myr and 10 Myr). This procedure nominally contains an error of ±30 °C (Laughland and Underwood 1993; Mukoyoshi et al. 2006).

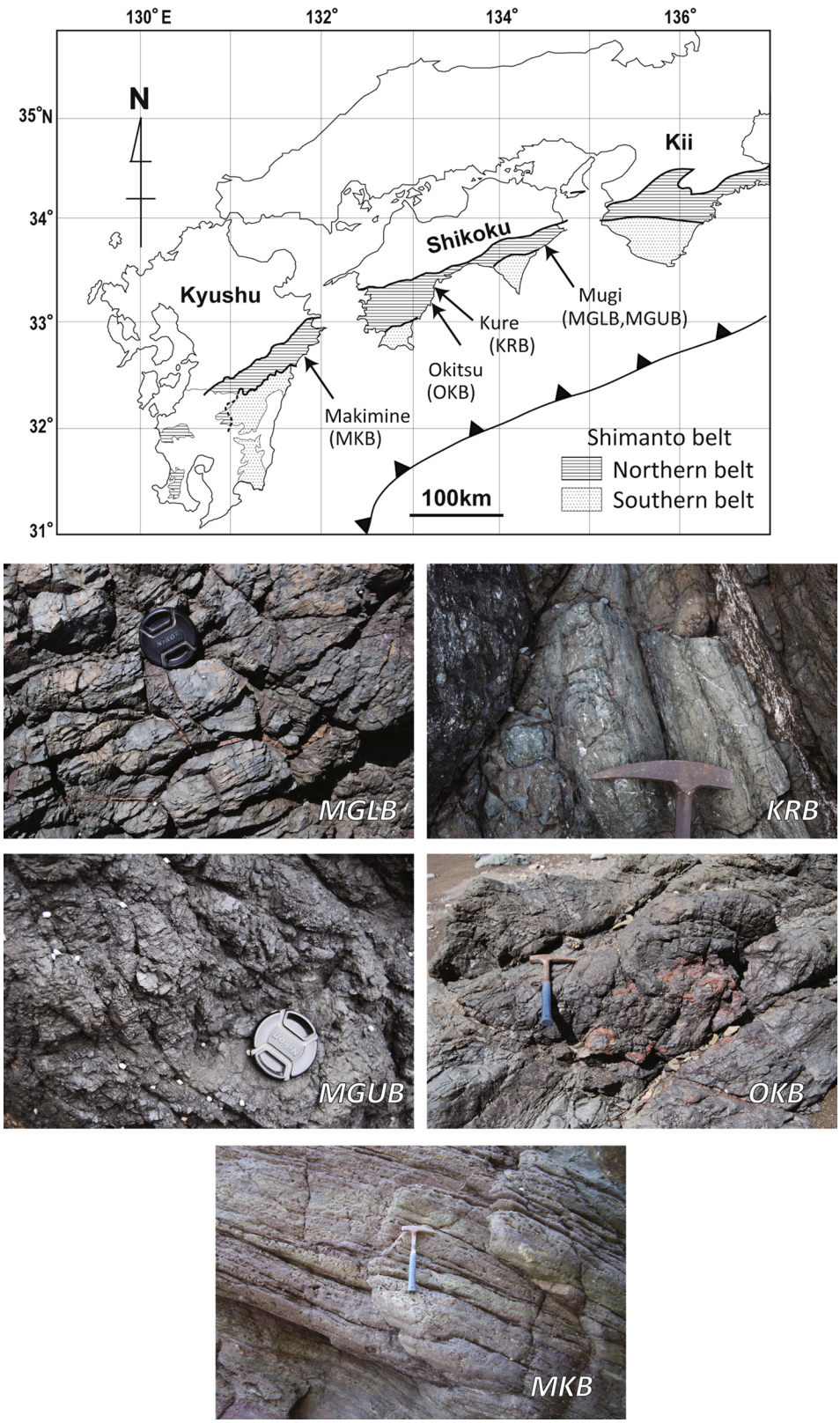

Fig. 1 Geological map of the Shimanto Belt in southwest Japan, showing the localities of mélange units that were sampled during this study and photographs of each sampling site

Table 1 Summary of the basalt samples analyzed during this study

Sample name	MGLB	KRB	MGUB	OKB	MKB	56R-1w[a]	54R-1w[a]
Sampling site	Mugi	Kure	Mugi	Okitsu	Makimine	Off the Kii	Off the Kii
V.R. (Ro)[b]	1.0	2.1	2.5	3.1	4.5		
1 (°C)	148	225	243	266	304		
2 (°C)	158	225	240	260	293		
3 (°C)	174	243	259	279	314		
4 (°C)	160 ± 30	230 ± 30	247 ± 30	268 ± 30	304 ± 30		
Quantitative rock composition							
Quartz	0.0	0.0	0.1	0.0	4.6	0.0	0.0
Plagioclase	45.1	37.1	44.0	47.0	42.4	38.0	39.3
Calcite	1.5	1.0	2.7	0.3	7.7	0.4	0.1
Pyroxene	24.1	27.5	20.2	19.1	0.0	24.4	22.9
Epidote	0.0	0.0	0.0	0.0	12.1	0.0	0.0
Fe oxide	2.1	5.9	5.7	1.9	2.4	3.7	1.5
Titanite	3.3	5.3	4.2	6.4	3.9	2.8	4.0
Total non-clays	76.1	76.8	76.8	74.8	73.1	69.2	67.9
Glass	0.0	0.0	0.0	0.0	0.0	7.1	8.1
Saponite	0.0	0.0	0.0	0.0	0.0	23.7	24.0
C/S	23.9	23.2	23.2	25.2	26.9	0.0	0.0
%S[c] in C/S	14.4	9.3	8.6	6.7	0.0	–	–
Total clay + glass	23.9	23.2	23.2	25.2	26.9	30.8	32.1
Total[d]	100 (93.1)	100 (102.8)	100 (100.3)	100 (102.2)	100 (103.3)	100 (97.3)	100 (90.0)
Chemical composition of C/S (based on $O_{10}(OH)_8$)							
N[e]	16	15	15	17	15		
Si	3.08 (0.23)	2.91 (0.12)	3.02 (0.12)	2.93 (0.10)	2.80 (0.14)		
$^{\Sigma}$Al	2.14 (0.16)	2.45 (0.16)	2.14 (0.15)	2.44 (0.12)	2.50 (0.12)		
^{IV}Al	0.92	1.09	0.98	1.07	1.20		
^{VI}Al	1.22	1.36	1.16	1.37	1.30		
Fe[f]	1.60 (0.26)	2.31 (0.21)	2.47 (0.24)	2.32 (0.29)	1.44 (0.28)		
Mg	2.73 (0.29)	2.11 (0.13)	2.05 (0.26)	2.12 (0.25)	3.11 (0.44)		
Ti	0.10 (0.12)	0.04 (0.05)	0.11 (0.06)	0.010 (0.23)	0.05 (0.04)		
Ca	0.12 (0.18)	0.01 (0.02)	0.02 (0.04)	0.00	0.00		

Temperatures for onland samples (1–4) were determined using (1) the equation of Barker (1988), (2) the equation of Sweeney and Burnham (1990) with a heating duration of 10 Myr, (3) the equation of Sweeney and Burnham (1990) with a heating duration of 1 Myr, and (4) averaged temperatures with an uncertainty of ±30 °C.
[a] Samples 54R-1w and 56R-1w were taken from intervals C0012-54R-1w (11–14 cm) and C0012-56R-1w (9–14 cm), respectively. [b] Vitrinite reflectance (V.R.) values for each sample are from Ikesawa et al. (2005) for samples MGLB and MGUB, from Mukoyoshi et al. (2006) for sample KRB, from Sakaguchi (1999) for sample OKB, and from Ohmori (1998) for sample MKB. [c] %S values were determined by clay-fraction XRD analysis. [d] Relative mineral abundances were determined using RockJock software and are normalized to 100% abundances. The total weight percentage values originally derived from the program are shown in parentheses. [e] N = number of analyzed grains with two standard deviations (2σ) shown in parentheses. [f] All Fe calculated as Fe^{2+}

The determined temperatures range from 160 ± 30 °C (MGLB) to 304 ± 30 °C (MKB).

Figure 2 shows the microtextures typical of the analyzed samples. Except for MKB, the samples comprise a framework of plagioclase and clinopyroxene phenocrysts (several hundreds of microns in size) with the spaces between them filled with fine-grained clay minerals. There is no visible trace of deformation in these samples. In contrast, sample MKB has been subjected to a bulk shear deformation, as represented by a strong foliation (Fig. 1).

In addition to these onland samples, and for comparative purposes, we analyzed the whole-rock mineralogy of ocean-floor basalt from the Shikoku Basin (samples 54R-1w and 56R-1w), recovered from Hole C0012B drilled during the Integrated Ocean Drilling Program (IODP) Expedition 322 (Saito et al. 2010). These two samples provide suitable reference material for the starting conditions of alteration just before basalt enters a subduction zone.

Laboratory methods

The samples were gently crushed, and unweathered fragments were carefully collected for mineralogical analysis. The fragments were dispersed ultrasonically in distilled water, and the clay fraction (<2.0 μm) of each sample was

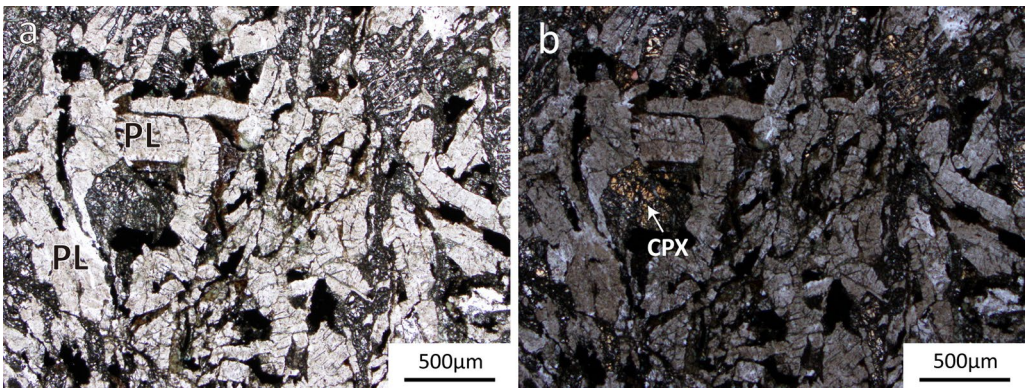

Fig. 2 Representative photomicrographs of intact pillow basalt (sample OKB) under plane-polarized (**a**) and cross-polarized (**b**) light; *PL* plagioclase, *CPX* clinopyroxene

separated with a centrifuge and dropped onto glass slides to prepare oriented mounts by air-drying in an oven at 60 °C (herein referred to as the "AD" (air-drying) state). These mounts were saturated with ethylene–glycol vapor overnight at 60 °C ("EG"). X-ray diffraction (XRD) patterns for the mounts were recorded using a Rigaku Rint-2000 with monochromatized CuK_α radiation at 40 kV and 30 mA, with 1° divergence and anti-scattering slits, and a 0.3-mm receiving slit in step scan mode for 6 s every 0.02° step in 2θ. Bulk powders, mixed with an internal standard (corundum, AX-5H, Hinomoto Kenmazai Co.) at a weight ratio of 4:1, were mounted by side loading to minimize the development of a preferred alignment of clay minerals and were X-rayed with the same instrumental setting. Bulk XRD patterns were quantitatively analyzed using RockJock software (Eberl 2003). A lack of appropriate data for mixed-layer clays meant that all patterns were tentatively analyzed using saponite and chlorite end-members, with mixed-layer clay abundances determined by summing the two end-member phases. The proportion of expandable layers (i.e., saponite) within the mixed-layer clays was analyzed using the method described by Hillier (1993; "Appendix"). The uncertainties involved in this approach are generally <5%. Peak processing (background subtraction, smoothing, and decomposition) was undertaken using the DECOMPXR peak decomposition software (Lanson 1997).

The clay-fraction powders were also dispersed on a holey film of carbon supported by a Cu grid for chemical analysis using an energy-dispersive X-ray spectrometer (EDX) in TEM (EX-24025JGT, Jeol). In order to minimize the loss of alkali elements (a significant issue when analyzing clay minerals), the beam diameter was extended to 200 nm while the counting duration was reduced to 30 s. Each grain was exposed to the electron beam with its c^* rotated by 20° from the beam axis toward the EDX detector. Quantitative chemical analyses were performed with *k* factors for O, Na, Mg, Al, Si, K, Ca, Ti, Mn, and Fe determined with standards of biotite, albite, olivine, and hornblende. Atomic ratios were obtained after correcting for the X-ray absorption of the specimen using the criterion of charge neutrality (Van Cappellen and Doukhan 1994).

Results

Figure 3 shows XRD patterns for bulk core (54R and 56R) and onland samples plotted as a function of increasing amounts of alteration. The lowermost four onland samples (MGLB, KRB, MGUB, and OKB) have almost identical XRD profiles that indicate they contain plagioclase, clinopyroxene, and clay minerals. Sample MKB contains epidote and calcite rather than clinopyroxene. The core samples recovered from the Shikoku Basin contain broad reflections at 6° 2θ that are indicative of the presence of saponite. The weight fractions of these constituent minerals were determined using RockJock software (Fig. 4; Table 1). The most abundant phase is plagioclase (ca. 40–45 wt%), followed by clinopyroxene (20–25 wt%), clay minerals (chlorite + saponite) (~25 wt%), and accessory titanite and Fe oxides. Sample MKB contains epidote (12 wt%) and calcite (8 wt%) but is free of clinopyroxene. In the RockJock analysis of the core samples, better fit was obtained between the experimental and modeled patterns when including the volcanic glass profile. The results indicate that the core samples both contain ~40 wt% plagioclase, ~25 wt% clinopyroxene, ~20 wt% saponite, and ~8 wt% volcanic glass (Fig. 4). Kameda et al. (2011a) also reported that the clay phase in these samples is discrete saponite without interstratified chlorite. In addition, these samples contain ~20 wt% bulk-rock saponite as evidenced by their cation exchange capacities (CEC) (Kameda et al. 2011a). This independent method yields clay content values that are comparable to the XRD analyses, indicating that the quantitative compositional data presented here are reliable.

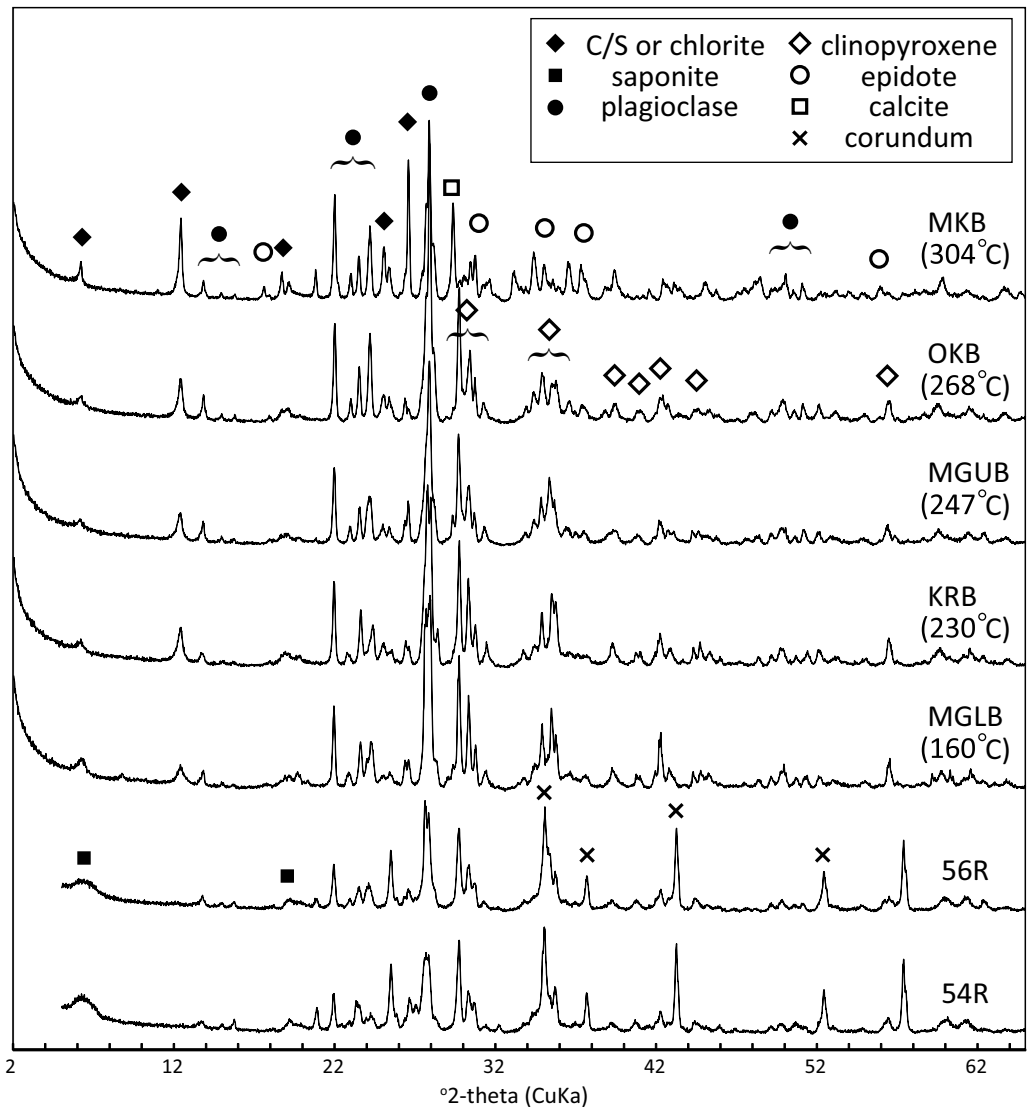

Fig. 3 Bulk XRD patterns for random powdered specimen mounts with sample abbreviations as per Fig. 1. The patterns of 54R-1w and 56R-1w are from ground powders mixed with corundum

The low 2θ angle profile (ca. <13°) within the bulk XRD patterns presented in Fig. 3 suggests that the crystallographic features of clay minerals change from sample to sample (Fig. 3). These variations were further analyzed using clay-fraction XRD, with the resulting patterns shown in air-dried (AD) and ethylene glycolated (EG) states in Fig. 5. Sharp peaks at 14 Å (6.2° 2θ) and 7.1 Å (12.5° 2θ) that are unresponsive to EG treatment suggest that sample MKB contains discrete chlorite. In comparison, the lower four onland samples contain a 31 Å peak (2.8°2θ) that is present in the EG state (depicted using arrows) and indicates that these samples contain a regularly interstratified 1:1 (or close to 1:1) mixed-layer chlorite–saponite (C/S) mineral called corrensite. Moreover, the peaks at 14 and 7.1 Å have complicated profiles that suggest these samples contain other C/S phases. Peak decomposition (Fig. 6; Table 2) suggests that these samples contain three C/S phases with different proportions of saponite layers. The peak migration curves for these samples (Fig. 9) suggest that the peaks at ~12.35°, ~12.2°, and ~11.5° correspond to C/S containing <5, ~10–20, and ~40% saponite layers, respectively. The C/S containing ~40% saponite layers has a structure very similar to that of corrensite, with the presence of this mineral also

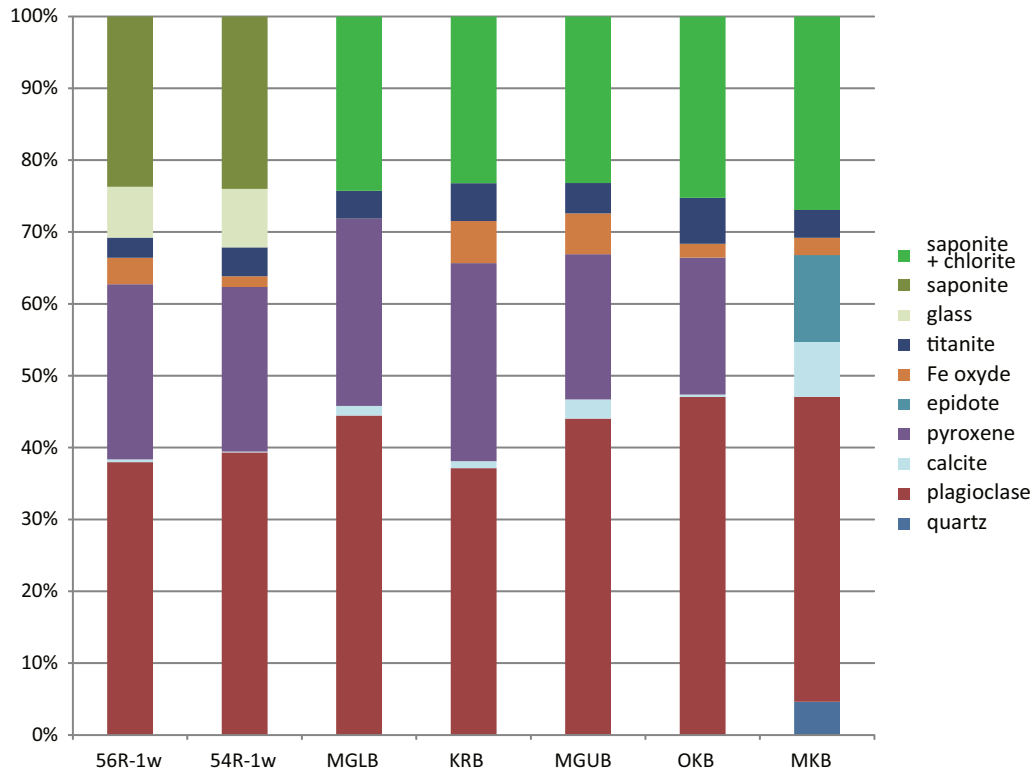

Fig. 4 Whole-rock mineral compositions determined using RockJock software. Data for core samples 56R-1w and 54R-1w are also shown

indicated by the 31 Å reflection described above. However, it is uncertain whether this peak is from discrete corrensite or is the result of segregated interstratification between chlorite and corrensite. One way to clarify this is by obtaining more precise C/S phase structures using specific XRD profile analysis (e.g., Drits et al. 2011).

The results outlined above allowed the net saponite fraction within the overall C/S phases (hereafter termed "%S") to be determined for each sample (Table 1). Sample MGLB has the highest %S value (14.4 %S), followed by samples KRB, MGUB, OKB, and MKB, an order that correlates with increasing alteration. In addition, the %S value for MKB is practically zero because the XRD pattern for this sample is indistinguishable from the ideal chlorite pattern (Fig. 5).

Table 1 summarizes C/S structural formulae (based on 14 oxygens) determined by TEM–EDX. The Ca within these samples is attributable to the interlayer cation within saponite layers. These Ca concentrations are consistent with the results of the XRD analysis described above (as exemplified by the sample with the highest Ca content, MGLB). More altered samples record an increase in Al and a decrease in Si that reflects the progressive chloritization of C/S (e.g., Scihffman and Staudigel 1995).

Discussion

Progressive chloritization in underthrust ocean-plate basalts within the seismogenic zone

This study has demonstrated an apparent correlation between progressive alteration (maximum burial temperature estimated by vitrinite reflectance) and changes in clay mineralogy despite nearly constant whole-rock mineral assemblages. These new data provide insights into the extent and pathways of alteration within subducting oceanic crustal material.

The core samples recovered from the Shikoku Basin provide a reference for the state of the oceanic basalt prior to subduction. Bulk XRD and CEC measurements by Kameda et al. (2011a) indicate that the uppermost ~40 m section of basalt within the basin is mineralogically homogeneous. This section is delineated by the presence of pore-filling saponite (~20 wt%) that formed during low-temperature alteration associated with seawater infiltration (e.g., Alt and Teagle 2003). The basalt also contains ~8 wt% volcanic glass (Fig. 4) that survived this low-temperature alteration but would have been altered to saponite during higher-temperature alteration. In contrast, the clay phases within the onland samples are present as either C/S (including corrensite) or discrete chlorite (MKB). Plotting the %S values for these

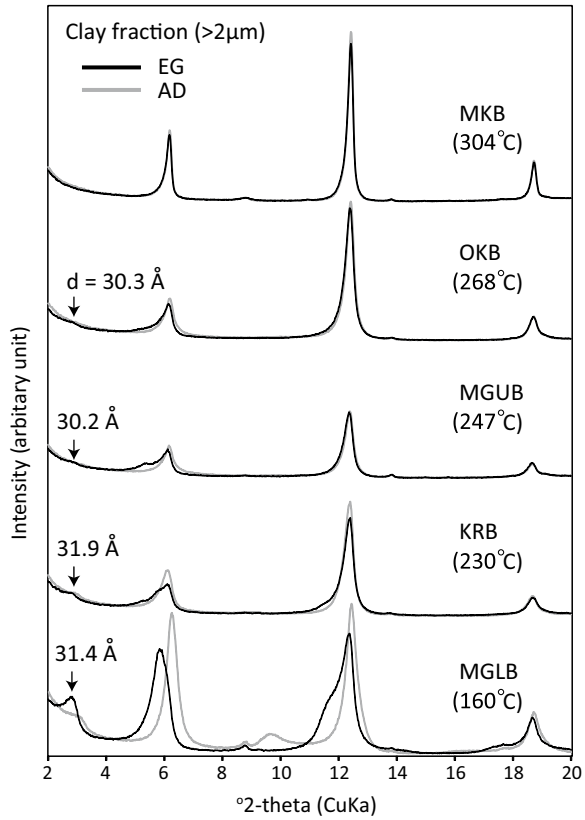

Fig. 5 XRD patterns for AD (*gray line*) and EG (*black line*) oriented mounts analyzed during this study. The peaks visible at ~31 Å correspond to the (001) reflection of corrensite

C/S phases against temperatures derived from vitrinite reflectance (Table 1) yields an inverse correlation (Fig. 7), with the steady decrease in %S explained by a progressive S–C reaction at depth within the subduction zone at temperatures up to >~300 °C. Although it could be possible that paleotemperatures estimated from vitrinite reflectance also represent original thermal maturation at various depth in the oceanic crust prior to subduction, temperatures more than 150 °C would be mainly attained during the formation of tectonic mélange along the plate interface, given the common thickness of trench-fill and hemipelagic sedimentary sequences at convergent margins (Underwood 2007). Although the S–C reaction has been observed in geological environments including in geothermal fields (Inoue and Utada 1991), within altered basalts or ophiolites (Alt and Teagle 2003), and within marine evaporites (Hillier 1993), our results demonstrated for the first time the successive conversion of S/C within the subducting oceanic crust along the seismogenic plate interface.

Sample MGLB contains the highest fraction of saponite layers (14 %S) of any of the onland samples. However, this value is less than half of the value obtained during previous research into pillow basalts from the same locality (Kameda et al. 2011c) (Fig. 7). This difference indicates significant variations in the extent of alteration within this area, even within the same basaltic units. One possibility for this difference is a retrogressive reaction (i.e., saponitization) by lower-temperature alteration during exhumation. The pillow basalt analyzed in the previous research is surrounded by a dense network of foliated cataclasites, suggesting an easier infiltration of low-temperature fluids after maximum burial, if faulting might have continued until the exhumation stage. The pillow basalt analyzed by Kameda et al. (2011c) contains fine-grained phenocrysts and is free of pyroxene, whereas sample MGLB was collected from more massive and undeformed part of the basalt body that contains larger phenocrysts and ~20 wt% pyroxene. This suggests that sample MGLB analyzed in present work is more similar to the onland and core samples used during this study compared with the sample described by Kameda et al. (2011c).

Clay-fraction XRD data suggest that saponite breaks down at ~300 °C (sample MKB; Fig. 7). Hillier (1993) reported that corrensite forms at 120–260 °C, a range of temperatures that is similar to the results presented in this study. Samples that formed at temperatures <~270 °C have almost constant whole-rock mineral assemblages, but these assemblages are modified at temperatures above ~300 °C, primarily as a result of the breakdown of pyroxene and the formation of epidote and incipient amphibole (Fig. 4). The presence of quartz would represent mobilization of SiO_2 from S–C reaction and/or infill from the surrounding rocks during progressive shearing.

Dehydration of underthrust basalts as a result of S–C conversion

The stable expansion and hydration of saponite interlayer spaces means that progressive S–C conversion can potentially enhance the bulk dehydration of underthrust oceanic basalts. This assumption seems feasible because in situ XRD experiments on the hydration state of Ca-saturated dioctahedral smectite (montmorillonite) have demonstrated that 15 Å hydration states (i.e., the two-layer hydrated form of the mineral) are stable up to 350 °C with little pressure dependence (Wu et al. 1997). Here, we consider that the saponite layer remains in this two-layer hydration state during alteration. The fact that chlorite is also hydrous means that the net amount of fluid expelled through S–C reactions is dependent on reaction stoichiometry. Using the chemical compositions of end-member saponite (Kameda et al. 2011a) and chlorite (MKB; Table 1) yields the following possible reaction:

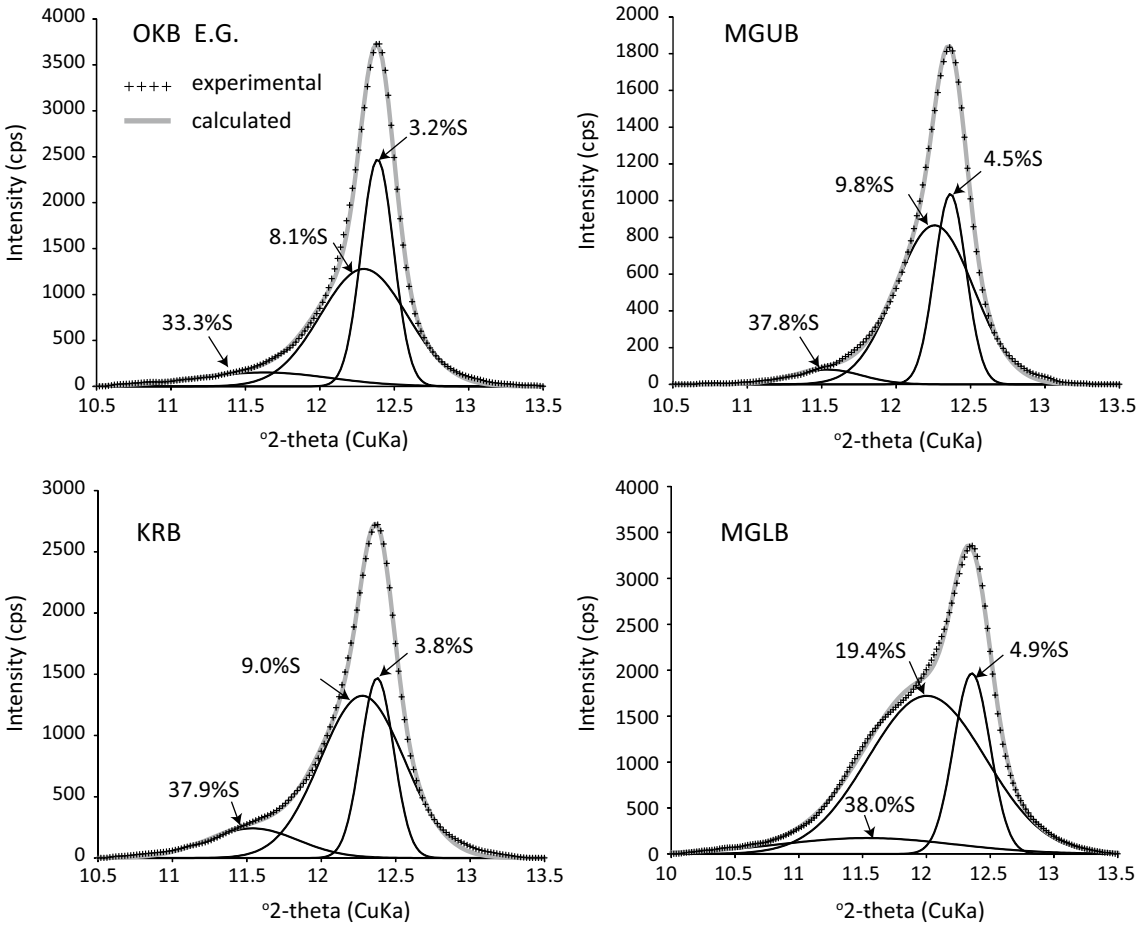

Fig. 6 Decomposition of the 7.1 Å C/S band of C/S within EG-treated samples; three peaks were used to fit the experimental profile. %S value for each decomposed peak from peak position and the working curve of Eq. (2) are also shown

Table 2 Results of peak decomposition for the 7.1 Å band

Sample	Peak 1				Peak 2				Peak 3			
	2θ	Intensity	FWHM	%S*	2θ	Intensity	FWHM	%S*	2θ	Intensity	FWHM	%S*
MGLB	12.35	1317	0.335	4.9	11.99	1147	1.085	19.4	11.52	115	1.616	38.0
KRB	12.37	988	0.257	3.8	12.27	884	0.665	9.0	11.53	161	0.717	37.9
MGUB	12.35	697	0.248	4.5	12.25	578	0.617	9.8	11.53	54	0.542	37.8
OKB	12.38	1661	0.254	3.2	12.29	853	0.687	8.1	11.62	100	1.046	33.3

* %S was estimated from 2θ of each decomposed peak with the working curve of Eq. (2)

$$\begin{aligned}&(Ca_{0.24}K_{0.074}Na_{0.02})\left(Al_{0.18}Fe_{1.18}Mg_{1.61}Ti_{0.02}\right)\\&\quad(Si_{3.22}Al_{0.78})O_{10}(OH)_2\cdot 4.5H_2O\ +\ 2.66H^+\\&\quad\rightarrow\ 0.77\left(R^{2+},\ Al_{0.65}\right)(Si_{1.40}Al_{0.60})O_5(OH)_4\\&\quad+\ \text{dissolved cations}\left(Ca^{2+},\ K^+,\ Na^+,\ Mg^{2+},\ Fe^{2+}\right)\\&\quad+\ 2.14SiO_2aq+5.29H_2O\end{aligned}\tag{1}$$

where R in the chlorite structural formula is the cation-occupying octahedral site. Equation (1) is constructed by considering that saponite contains two layers of interlayer water (i.e., 4.5 mol of water per structural formula of smectite based on the basal spacing as well as water density; Ransom and Helgeson 1994), with a factor of 0.77 for chlorite adopted to balance the amount of immobile Al present during this reaction. This reaction corresponds to

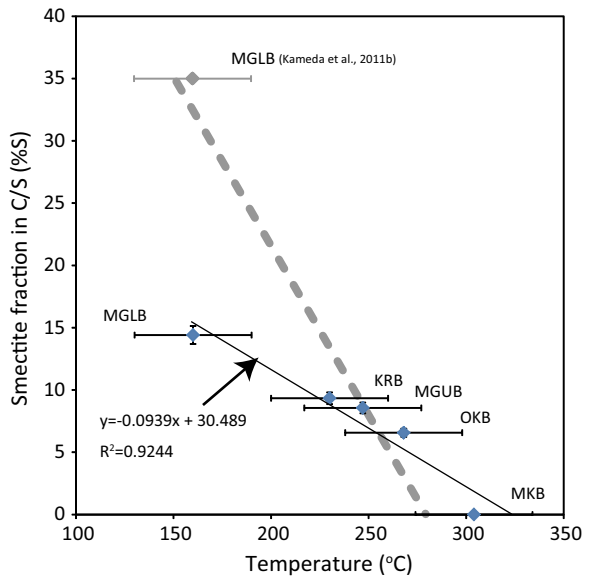

Fig. 7 Variations in %S values as a function of temperature with horizontal and vertical error bars of ±30 °C (Laughland and Underwood 1993) and ±5% (Hillier 1993), respectively. The diagram also shows variations in saponite content within sample MGLB as determined by Kameda et al. (2011a). The conversion reaction rate reported by Kameda et al. (2011c) is shown as a *dotted gray line*

a processes proposed by Bettison-Varga and Mackinnon (1997) that leads to the release of fluids, thus contributing to the bulk dehydration of oceanic basalts.

Here, we use the Nankai subduction zone as a case study to examine the possible dehydration of underthrusting basalts. Unlike sedimentary smectite-to-illite (S–I) conversion reactions, there is no appropriate kinetic equation for the S–C reaction, meaning that we use a simplified situation where %S decreases linearly from 14 to 0%S with increasing temperature (160–300 °C) along the plate interface (Fig. 7). It should be noted that the samples analyzed during this study most likely spent a great deal of time at or near their peak temperature prior to exhumation. This means that reactions may have progressed further in these rocks than would be the case for active prograde settings where kinetics would limit reaction progress as a result of rapid movement through temperature space. The implicit assumption of equilibrium also means that these reaction rates should be considered maxima, with dehydration most likely persisting to even greater depths and temperatures higher than 300 °C as a result of kinetic effects.

The numerical modeling presented by Peacock and Wang (1999) demonstrated that the horizontal distance for completion of the 14–0%S conversion reaction (i.e., a change in temperature from 160 to 300 °C along a décollement) is ~70 km. Spinelli and Wang (2008) indicated that this change occurred over a distance of ~60–90 km along the Muroto transect within the Nankai margin, depending on the effect of hydrothermal circulation on the oceanic crust. The relative convergence rate of 68 km/Myr at the Nankai margin (=plate convergence rate + prism outbuilding rate; Saffer et al. 2008) means that this reaction will take ~1.0 Myr to complete. Combining the bulk-rock C/S volume fraction (0.24; Table 1) with the volume fraction of water within the saponite interlayer (0.4; Kameda et al. 2011a) and a bulk-rock porosity of 5% (Kato et al. 2004), Eq. (1) suggests that the average release rate of water per unit volume of basalt for 1.0 Myr (V_{H_2O}/V_{ROCK} t^{-1}) = 0.14 (saponite layer fraction in C/S) × 0.24 (volume fraction of C/S in bulk rock) × 0.40 (volume fraction of interlayer water in saponite) × 0.95 (solid volume fraction of basalt rock) × 5.29/4.50 [volume ratio between the released and contained water in saponite interlayer from Eq. (1)] = ~0.015 Myr^{-1} = ~0.48 × 10^{-15} s^{-1}. This dehydration rate is lower than is suggested by previous research (Kameda et al. 2011a), primarily as a result of overestimation of the %S within the S–C in sample MGLB as well as the geothermal structure of the subduction zone (i.e., variations in reaction rate), with the down-dip limit of the dehydration window extending to >300 °C (Fig. 7). However, it is noted that the above dehydration rate is almost equal to, or greater than those from the underplated sediments (~10^{-15}–<10^{-16} s^{-1}) estimated by Saffer et al. (2008). The fact that oceanic basalts are exposed on the upper surface of the subducting plate in an area of duplex underplating means that S–C reactions are thought to be an important source of fluid for the plate-boundary fault system. Yamaguchi et al. (2012) determined the $\delta^{18}O$ and $^{87}Sr/^{86}Sr$ values of several types of crack-fill veins associated with basalts in the Mugi mélange and used these data to suggest that the fluids that formed these veins were strongly influenced by basalt buffered fluids, a finding that is consistent with the bulk oceanic basalt dehydration processes identified during this study. The fluids resulting from basalt dehydration may also widely circulate within the mélange and can form pervasive sets of mineral veins within the seismogenic zone (Hashimoto et al. 2012).

Influence of oceanic crust dehydration on décollement step-down

Dehydration within low-permeability environments can disturb the hydrological and mechanical states in and around the dehydrating body as well as the dynamic aspects of deformation. Kato et al. (2004) examined the permeability of exhumed basalt around an ancient subduction zone thrust (namely altered basalt within the Okitsu mélange) and reported values of 10^{-19}–10^{-20} m^2.

Several massive basalt samples from the Shimanto belt yielded even lower values of 10^{-21}–10^{-22} m^2 under confining pressures of ~100 MPa (Tanikawa, unpublished data). The dehydration and steady outflow of fluid through subducting oceanic basalts under these low-permeability conditions may result in overpressure within the dehydrating basalt layer. The Mugi mélange contains crack-filling extensional veins that are pervasively developed just above the basalt (Yamaguchi et al. 2012). Since these veins are mostly extensional (filled with mode I cracks), the fluid pressure is higher than σ_3 plus tensile strength of the mélange, suggesting that these veins formed as a result of overpressuring of the underlying basalt.

Overpressure will also be enhanced within the dehydrating basalt, potentially generating a weaker and more deformable layer relative to the surrounding units as a result of a decrease in effective stress. Concurrently, the sedimentary décollement may be progressively hardened by ongoing quartz veining and/or cementation (Kameda et al. 2014), a process that can cause a strength reversal and the fracturing and breakage of the basalt. This breakage will cause the fracture zone to propagate as a major thrust fault (i.e., a "step-down" of the décollement into the oceanic crust; Kimura and Ludden 1995; Ikesawa et al. 2005), leading to underplating of the upper section of the oceanic crust and the incorporation of this material into the overriding accretionary prism. Kimura and Ludden (1995) suggested that onland accretionary complexes contain accreted ocean-plate basalts of a few meters to ~300 m thick. These authors also suggested that these variations in thickness reflect the original hydrological profile of the oceanic crust prior to subduction, with relatively porous and permeable sections below the upper ~100 m of pillow basalts, with lower permeabilities as a result of pore-filling precipitates such as clays and volcanic glass potentially acting as weaker and more easily fractured horizons (Kimura and Ludden 1995). However, it is uncertain whether these hydrological systems actually exist, even at depth within subduction zone environments.

The deepest drillhole into the igneous oceanic crust (ODP Site 504B; Alt et al. 1996) contains discrete saponite to a depth of ~600 m from the top of the basement material that is capable of dehydration. The clay phases within deeper portions of this drillhole were originally mixed-layer C/S or chlorite, meaning that these deeper sections are unlikely to have undergone bulk dehydration. Although the bulk-rock saponite content of the samples obtained during this drilling was not determined, some 20–40 wt% of saponite was identified within the upper 70 m of basement section (i.e., depth from the bottom of the hole upward) of the pre-subduction Cocos Plate at the Costa Rica margin (Kameda et al. 2015). This suggests that breakage can occur within this saponite-bearing dehydrating section, triggered by dehydration-induced weakening of the oceanic crust.

This process should be quantitatively assessed by modeling using appropriate experimental porosity data and information on the permeability evolution of dehydrating basalt. The results would also provide insights into variations in the thickness of exposed onland basaltic fragments.

Implications for plate-boundary seismogenesis

The underplating of oceanic crust is most likely linked to plate-boundary seismogenic processes. Basalt breakage occurs within intact grain-supported pillow basalts (Fig. 2). Although the frictional property of basalt has yet to be tested, laboratory friction experiments demonstrated that materials dominated by framework minerals such as feldspar have higher frictional strength but velocity-weakening properties that allow the nucleation of seismic ruptures during fracturing (e.g., Ikari et al. 2011) (Fig. 8). However, the lateral extension of plate-boundary faults is associated with mature fault rocks such as foliated cataclasite and ultracataclasite that are present in underplated oceanic basalts (Ikesawa et al. 2005; Ujiie et al. 2007). Ultracataclasite layers contain fine-grained fragments of plagioclase and pyroxene within a clay matrix (Ujiie et al. 2007; Kameda et al. 2011c), and these matrix-supported and clay-dominated fault rocks contrast with intact basalts in that they probably have low shear strengths but may undergo velocity strengthening that means they do not undergo slip instability (e.g., Saffer and Marone 2003; Fig. 8). Ujiie et al. (2007) documented ultracataclasites with textures indicative of the fluidization of granular materials and the injection of this fluidized material into the host rock, possibly as a result of thermally activated pressurization during high-velocity frictional slip. This type of thermal pressurization is evidenced by the presence of stretched fluid inclusions in calcite veins (Ujiie et al. 2008) and progressed chloritization within the ultracataclasite layer (Kameda et al. 2011c). These observations suggest that faults can be dynamically weakened to assist the propagation of co-seismic slip under fluid-infiltrated conditions (Fig. 8), with the majority of these fluids generated by the dehydration of oceanic basalt. It is noted that these fault rocks contain more abundant clays than the intact and/or weakly deformed basalts, and the amount/rate of dehydration described above will be more significant along the faults.

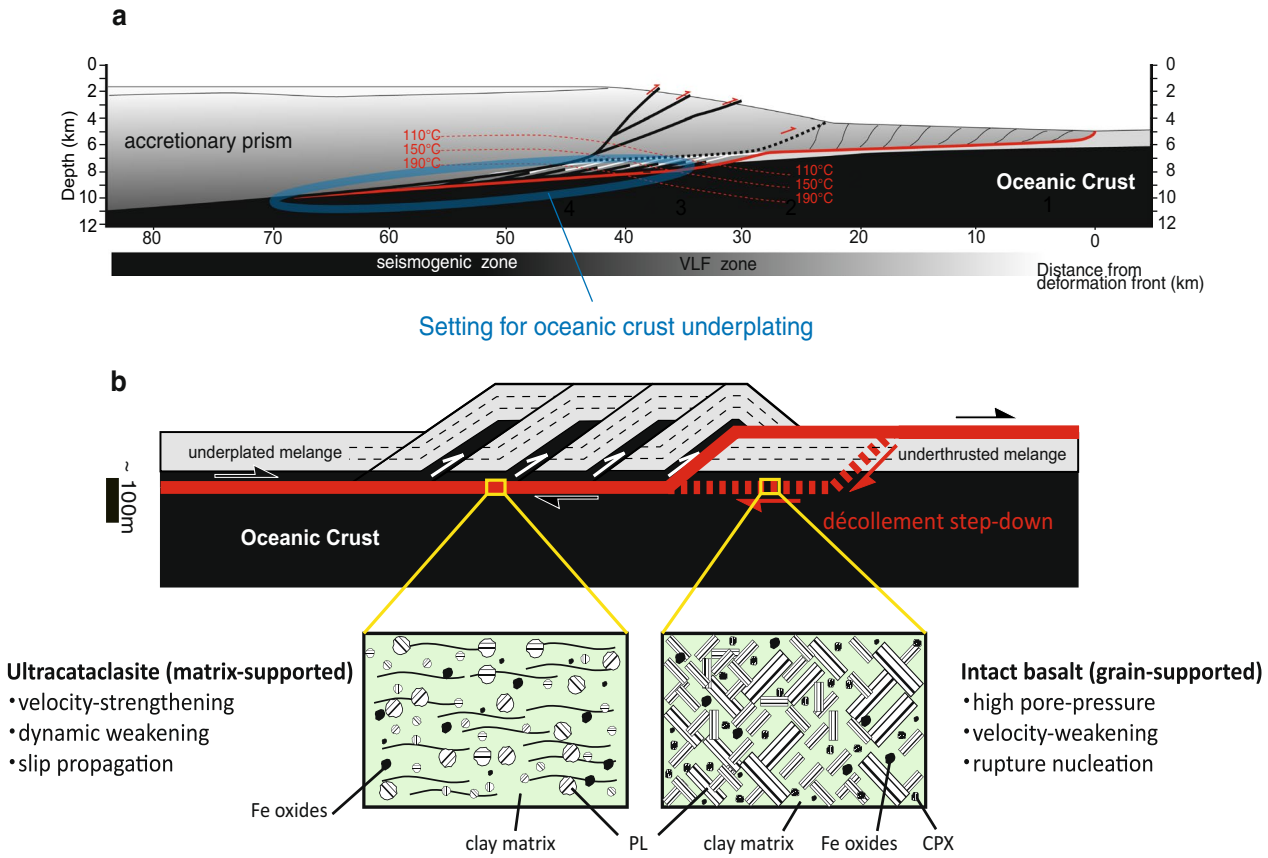

Fig. 8 Model showing **a** the setting for décollement step-down at the plate interface, and **b** the textural evolution from intact basalt to mature fault rock (ultracataclasite) as observed in onland exposures. The *diagram* also shows expected frictional properties and behaviors associated with seismogenesis. *Abbreviations* are as in Fig. 2

As mentioned above, Matsumura et al. (2003) suggested that the site for the initiation of décollement step-down is almost coincident with the location of seismogenesis. This means that the seismogenic fracturing of oceanic basalt near the up-dip limit of the seismogenic zone could nucleate seismic ruptures to propagate along dynamically weakened plate-boundary faults. Our results also predict that dehydration-induced breakage of basalt can persist up to temperatures of >~300 °C, implying that this breakage can result in seismogenic faulting at great focal depths.

Conclusions

This research focuses on the alteration and dehydration of subducting oceanic crust and presents new mineralogical data for pillow basalts within the Shimanto belt as well as core samples recovered from the basement of the Shikoku Basin. Our XRD analysis suggests that the onland samples contain clay minerals that are dominated by mixed-layer C/S minerals (including corrensite). In addition, the saponite–chlorite conversion within C/S steadily progresses with increasing alteration of the host basalt rock. This alteration reaction can supply mineral-bound water at a rate of 0.48×10^{-15} s^{-1} to seismogenic plate interfaces at temperatures >~300 °C. We hypothesize that basalt dehydration can also cause the weakening and eventual breakage of the basalt itself, generating a seismogenic décollement step-down. Although this tentative scenario needs to be verified using more quantitative hydrological modeling and realistic hydration property of expandable saponite layers, it is supported by several lines of geological evidence including variations in the thickness of basalt slabs embedded in the Shimanto belt as well as the geochemistry of mineralized veins around these slabs.

Authors' contributions

JK, WT, AY, YH, and GK designed this study. JK, AY, and YH carried out field survey and sampling. JK and SI conducted the mineralogical analysis and description. JK drafted the main manuscript and prepared the figures. All authors read and approved the final manuscript.

Author details
[1] Department of Natural History Sciences, Graduate School of Science, Hokkaido University, N10 W8, Sapporo 060-0810, Japan. [2] Department of Geosciences, Virginia Polytechnic Institute and State University, Blacksburg, VA 24061, USA. [3] Kochi Institute for Core Sample Research, Japan Agency for Marine-Earth Science and Technology, Nankoku 783-8502, Japan. [4] Atmosphere and Ocean Research Institute, The University of Tokyo, 5-1-5 Kashiwanoha, Kashiwa, Chiba 277-8564, Japan. [5] Department of Applied Science, Faculty of Science, Kochi University, Akebonocyo 2-5-1, Kochi 780-8520, Japan. [6] Tokyo University of Marine Science and Technology, Konan, Minato-ku, Tokyo 108-8477, Japan.

Acknowledgements
This research used samples and data provided by IODP (http://www.iodp.org/). DECOMPXR was kindly provided by B. Lanson. We thank two anonymous reviewers for valuable comments and Editor Toru Takeshita for editing this paper. This work was supported by JSPS Grants-in-Aid for Scientific Research on Innovative Areas (21107005 and 26109004) and JSPS KAKENHI Grant (15H03746).

Competing interests
The authors declare that they have no competing interests.

Appendix

Estimation of saponite layer fraction in mixed-layer C/S (%S)

The %S values of the clay phases in each sample were estimated using the approach outlined by Hillier (1993), where peak migration curves derived by Hower (1981) were used for regularly ordered (R = 1; i.e., free of any successive saponite–saponite pairs within stacking %S < 50) C/S for peaks between 8.5 and 7.1 Å. We used working curves for C/S with Fe = 2.0 (based on 14 oxygens) that are relevant for our samples using a 1-D XRD pattern calculation program (NEWMOD; Reynolds Jr 1985). The 7.1 Å peak of C/S with %S values of 50–100% was produced at a 5%S step, with the polynomial fit of the results yielding two expressions for the peak position versus %S, and %S versus relative peak intensity (RI) relationships (Fig. 9), as follows:

$$y = 45.53 \times x^3 - 1631.34 \times x^2 + 19514.36 \times x - 77860.50 \quad (2)$$

$$y = 0.00000629 \times x^3 - 0.000603 \times x^2 - 0.0194 \times x + 2.675, \quad (3)$$

where RI indicates the peak intensity relative to the peak intensity for 100%S. These curves were used to estimate %S values from peak position data and to estimate mass ratios between multiple C/S phases with different %S values from corrected peak intensities.

Publisher's Note

Received: 20 January 2017 Accepted: 6 April 2017
Published online: 18 April 2017

References

Alt JC, Teagle DAH (2003) Hydrothermal alteration of upper oceanic crust formed at a first spreading ridge: mineral, chemical, and isotope evidence from ODP Site 801. Chem Geol 201:191–211

Alt JC, Vanko D, Tartarotti P, Teagle DAH, Bach W, Zuleger E, Erzinger J, Honnorez J, Pezard PA, Becker K, Salisbury MH, Wilkens RH (1996) Hydrothermal alteration of a section of upper oceanic crust in the eastern equatorial Pacific: a synthesis of results from Site 504DSDP legs 69, 70, and 83, and ODP legs 111, 137, 140, and 148. In: Alt JC, Kinoshita H, Stokking L, Michael P (eds) ODP proceedings. Scientific results, vol 148. Ocean Drilling Program, College Station, pp 417–434

Barker CE (1988) Geothermics of petroleum systems: implication of the stabilization of kerogen thermal maturation after a geologically brief heating duration at peak temperature. US Geol Surv Bull 1870:26–29

Bettison-Varga L, Mackinnon IDR (1997) The role of randomly mixed-layered chlorite/smectite in the transformation of smectite to chlorite. Clay Clay Miner 45:506–516. doi:10.1346/CCMN.1997.0450403

Drits VA, Ivanovskaya TA, Sakharov BA, Zviagina BB, Gor'kova NV, Pokrovskaya EV, Savichev AT (2011) Mixed-layer corrensite-chlorites and their formation mechanism in the glauconitic sandstone-clayey rocks (Riphean, Anbar uplift). Lithol Miner Resour 6:635–665

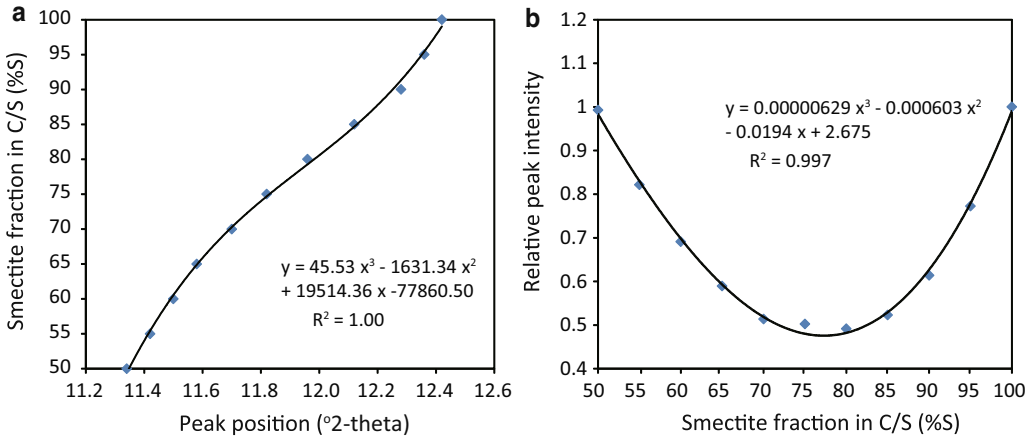

Fig. 9 Results of the NEWMOD calculations undertaken to derive polynomial expressions for the **a** peak position versus %S and **b** %S vs. relative peak intensity (RI) relationships.

Eberl DD (2003) User's guide to RockJock-A program for determining quantitative mineralogy from powder X-ray diffraction data. USGS Open-file report 03-78

Hacker BR, Simon M, Peacock SM, Abers GA, Holloway SD (2003) Subduction factory 2. Are intermediate-depth earthquakes in subducting slabs linked to metamorphic dehydration reactions? J Geophys Res 108:2030. doi:10.1029/2001JB001129

Hashimoto Y, Kimura G (1999) Underplating process from mélange formation to duplexing: example from the Cretaceous Shimanto Belt, Kii Peninsula, southwest Japan. Tectonics 18:92–107. doi:10.1029/1998TC900014

Hashimoto Y, Eida M, Kirikawa T, Iida R, Takagi M, Furuya N, Nikaizo A, Kikuchi T, Yoshimitsu T (2012) Large amount of fluid migration around shallow seismogenic depth preserved in tectonic mélange: Yokonami mélange, the Cretaceous Shimanto Belt, Kochi, Southwest Japan. Isl Arc 21:53–64

Hillier S (1993) Origin, diagenesis, and mineralogy of chlorite minerals in Devonian lacustrine mudrocks, Orcadian basin, Scotland. Clays Clay Miner 41:240–259

Hower J (1981) X-ray diffraction identification of mixed-layer clay minerals. In: Longstaffe FJ (ed) Clays and the resource geologist. Mineralogical Association of Canada short course handbook, vol 7. Mineralogical Association of Canada, Calgary, Alberta, pp 39–59

Hyndman RD (2007) The seismogenic zone of subduction thrust faults: what we know and don't know. In: Dixon T, Moore J (eds) The seismogenic zone of subduction thrust faults. Colombia University Press, New York, pp 15–41

Ikari MJ, Marone C, Saffer DM (2011) On the relation between fault strength and frictional stability. Geology 391:83–86

Ikesawa E, Sakaguchi A, Kimura G (2003) Pseudotachylyte from an ancient accretionary complex: evidence for melt generation during seismic slip along a master décollement? Geology 31:637–640. doi:10.1130/0091-7613

Ikesawa E, Kimura G, Sato K, Ikehara-Ohmori K, Kitamura Y, Yamaguchi A, Ujiie K, Hashimoto Y (2005) Tectonic incorporation of the upper part of oceanic crust to overriding plate of a convergent margin: an example from the Cretaceous-early Tertiary Mugi Mélange, the Shimanto Belt, Japan. Tectonophysics 401:217–230

Imai I, Teraoka Y, Okumura K (1971) Geologic structure and metamorphic zonation of the northeastern part of the Shimanto terrane in Kyushu, Japan. J Geol Soc Jpn 77:207–220

Inoue A, Utada M (1991) Smectite-to-chlorite transformation in thermally metamorphosed volcanoclastic rocks in the Kamikita area, northern Honshu, Japan. Am Miner 76:628–640

Kameda J, Yamaguchi A, Saito S, Sakuma H, Kawamura K, Kimura G (2011a) A new source of water in seismogenic subduction zones. Geophys Res Lett 38:L22306. doi:10.1029/2011GL048883

Kameda J, Raimbourg H, Kogure T, Kimura G (2011b) Low-grade metamorphism around the down-dip limit of seismogenic subduction zones: example from an ancient accretionary complex in the Shimanto Belt, Japan. Tectonophysics 502:383–392

Kameda J, Ujiie K, Yamaguchi A, Kimura G (2011c) Smectite to chlorite conversion by frictional heating along a subduction thrust. Earth Planet Sci Lett 305:161–170. doi:10.1016/j.epsl.2011.02.051

Kameda J, Kawabata K, Hamada Y, Yamaguchi A, Kimura G (2014) Quartz deposition and its influence on the deformation process of megathrusts in subduction zones. Earth Planets Space 66:13. doi:10.1186/1880-5981-66-13

Kameda J, Harris RN, Shimizu M, Ujiie K, Tsutsumi A, Ikehara M, Uno M, Yamaguchi A, Hamada Y, Namiki Y, Kimura G (2015) Hydrogeological responses to incoming materials at the erosional subduction margin, offshore Osa Peninsula, Costa Rica. Geochem Geophys Geosys. doi:10.1002/2015GC005837

Kato A, Sakaguchi A, Yoshida S, Yamaguchi H, Kaneda Y (2004) Permeability structure around an ancient exhumed subduction-zone fault. Geophys Res Lett 31:L06602. doi:10.1029/2003GL019183

Kiminami K, Miyashita S, Kawabata K (1994) Ridge collision and in situ greenstones in accretionary complexes: an example from the Late Cretaceous Ryukyu Islands and southwest Japan margin. Isl Arc 3:103–111

Kimura G, Ludden J (1995) Peeling oceanic crust in subduction zones. Geology 23:217–220. doi:10.1130/0091-7613(1995)023b0217:POCISZ>2.3.CO;2

Kimura G, Mukai A (1991) Underplated units in an accretionary complex: mélange of the Shimanto belt of eastern Shikoku, southwest Japan. Tectonics 10:31–50. doi:10.1029/90TC00799

Kimura G, Yamaguchi A, Hojo M, Kitamura Y, Kameda J, Ujiie K, Hamada Y, Hamahashi M, Hina S (2012) Tectonic mélange as fault rock of subduction plate boundary. Tectonophysics 568–569:25–38

Lanson B (1997) Decomposition of experimental X-ray diffraction patterns (profile fitting): a convenient way to study clay minerals. Clays Clay Miner 45:132–146

Laughland M, Underwood MB (1993) Vitrinite reflectance and estimates of paleotemperature within the Upper Shimanto Group, Muroto Peninsula, Shikoku, Japan. In: Underwood MB (ed) Thermal evolution of the tertiary Shimanto Belt, Southwest Japan: an example of Ridge–Trench interaction. Geological Society of America, special paper, vol 273, pp 25–43

Matsumura M, Hashimoto Y, Kimura G, Ohmori-Ikehara K, Enjoji M, Ikesawa E (2003) Depth of oceanic crust underplating in subduction zone-inference from fluid inclusion analysis of crack-seal vein. Geology 31:1005–1008

Mori K, Taguchi K (1988) Examination of the low-grade metamorphism in the Shimanto Belt by vitrinite reflectance. Mod Geol 12:325–339

Mukoyoshi H, Sakaguchi A, Otsuki K, Hirono T, Soh W (2006) Co-seismic frictional melting along an out-of-sequence thrust in the Shimanto accretionary complex. Implications on the tsunamigenic potential of splay faults in modern subduction zones. Earth Planet Sci Lett 245:330–343. doi:10.1016/j.epsl.2006.02.039

Ohmori K (1998) Paleothermal structure and tectonic evolution of the Shimanto accretionary prism, Southwest Japan. Ph.D. thesis, University of Tokyo

Ohmori K, Taira A, Tokuyama H, Sakaguchi A, Okamura M, Aihara N (1997) Paleothermal structure of the Shimanto accretionary prism, Shikoku Japan: role of an out-of-sequence thrust. Geology 25:327–330. doi:10.1130/0091-7613(1997)025b0327:PSOTSA>2.3.CO;2

Park JO, Tsuru T, Takahashi N, Hori T, Kodaira S, Nakanishi A, Miura S, Kaneda Y (2002) A deep strong reflector in the Nankai accretionary wedge from multichannel seismic data: implications for underplating and interseismic shear stress release. J Geophys Res 107:2061. doi:10.1029/2001JB000262

Peacock SM, Wang K (1999) Seismic consequences of warm versus cool subduction metamorphism: examples from southwest and northeast Japan. Science 286:937–939

Ransom B, Helgeson HC (1994) A chemical and thermodynamic model of aluminous dioctahedral 2:1 layer clay minerals in alteration processes: regular solution of representation of interlayer dehydration in smectite. Am J Sci 294:449–484. doi:10.2475/ajs.294.4.449

Reynolds RC Jr (1985) *NEWMOD* a computer program for the calculation of one-dimensional diffraction patterns for mixed-layered clays. RC Reynolds 8 Brook Rd, Hanover, New Hampshire

Saffer DM, Marone C (2003) Comparison of smectite- and illite-rich gouge frictional properties: application to the updip limit of the seismogenic zone along subduction megathrusts. Earth Planet Sci Lett 215:219–235

Saffer DM, Tobin HJ (2011) Hydrogeology and mechanics of subduction zone forearcs: fluid flow and pore pressure. Ann Rev Earth Planet Sci 39:157–186

Saffer DM, Underwood MB, McKiernan AW (2008) Evaluation of factors controlling smectite transformation and fluid production in subduction zones: application to the Nankai Trough. Isl Arc 17:208–230. doi:10.1111/j.1440-1738.2008.00614.x

Saito S, Underwood MB, Kubo Y, the Exp 322 Scientists (2010) Proc IODP 322, Tokyo (Integrated Ocean Drilling Program Management International, Inc.). doi:10.2204/iodp.proc.322.2010

Sakaguchi A (1996) High paleogeothermal gradient with ridge subduction beneath the Cretaceous Shimanto accretionary prism, southwest Japan. Geology 24:795–798. doi:10.1130/0091-7613(1996)024b0795:HPGWRS>2.3.CO;2

Sakaguchi A (1999) Thermal structure and paleo-heat flow in the Shimanto accretionary prism, Southwest Japan. Isl Arc 3:359–372. doi:10.1046/j.1440-1738.1999.00246.x

Scihffman P, Staudigel H (1995) The smectite to chlorite transition on a fossil seamount hydrothermal system: the basement complex of La Palma, Canary Islands. J Metamorph Geol 13:487–498

Silver EA, Ellis MJ, Breen NA, Shipley TH (1985) Comments on the growth of accretionary wedges. Geology 13:6–9

Spinelli GA, Wang K (2008) Effects of fluid circulation in subducting crust on Nankai margin seismogenic zone temperatures. Geology 36:887–890
Sweeney JJ, Burnham AK (1990) Evaluation of a simple model of vitrinite reflectance based on chemical kinetics. Am Ass Petrol Geol Bull 74:1559–1570
Taira A, Katto M, Okamura M, Kodama K (1988) The Shimanto Belt in Shikoku, Japan evolution of Cretaceous to Miocene accretionary prism. Mod Geol 12:5–46
Ujiie K, Yamaguchi A, Kimura G, Toh S (2007) Fluidization of granular material in a subduction thrust at seismogenic depths. Earth Planet Sci Lett 259:307–318
Ujiie K, Yamaguchi A, Taguchi S (2008) Stretching of fluid inclusions in calcite as an indicator of frictional heating on faults. Geology 36:111–114
Underwood MB (2007) Sediment input to subduction zones: why lithostratigraphy and clay mineralogy matter. In: Dixon T, Moore JC (eds) The seismogenic zone of subduction thrust faults. Colombia University Press, New York, pp 15–41
Van Cappellen E, Doukhan JC (1994) Quantitative transmission X-ray microanalysis of ionic compounds. Ultramicroscopy 53:343–349
Wu TC, Bassett WA, Huang WL, Guggenheim S, Koster van Groos AF (1997) Montmorillonite under high H_2O pressures: stability of hydrate phases. Rehydration hysteresis, and the effect of interlayer cations. Am Miner 82:69–78
Yamaguchi A, Ujiie K, Nakai S, Kimura G (2012) Sources and physicochemical characteristics of fluids along a subduction-zone megathrust: a geochemical approach using syn-tectonic mineral veins in the Mugi mélange, Shimanto accretionary complex. Geochem Geophys Geosys 13:Q0AD24. doi:10.1029/2012GC004137